ACS OMEGA

http://pubs.acs.org/journal/acsodf

Article

Tetrathiafulvalene–Benzothiadiazole: A Metal-Free Photocatalyst for Hydrogen Production

Hajar Mahmoudi,* Abdel El Kharbachi,* Hassan Safari, and Abbas Ali Jafari

Cite This: *ACS Omega* 2022, 7, 42283–42291

Read Online

ACCESS | Metrics & More | Article Recommendations | Supporting Information

ABSTRACT: In this work, a series of hybrid tetrathiafulvalene–benzothiadiazole (TTF–BTD) are designed and applied as a metal-free photocatalyst for hydrogen production, particularly under visible light irradiation. Density functional theory calculations are used to shed light on the photophysical properties observed in the various TTF–BTD derivatives and investigated by the obtained data. Because band gap engineering has normally been used as an effective approach, we studied the effect of the various functional groups on the band gap to set a favorable band alignment with photocatalysts. An increase in highest occupied molecular orbital and lowest unoccupied molecular orbital energy levels is observed in the order CH_3 < Br < CF_3 < COOMe < CN. The results discover that COOMe-TTF-CN-BTD can have a clear photocatalytic potential in the hydrogen production for specific applications. Our experimental and theoretical studies reveal that the CN-withdrawing group increases the reduction potential of the conduction band; meanwhile, COOMe decreases the reduction potential of the valance band. Moreover, we demonstrate that H_2O reduction and oxidation reaction energies are both located inside the COOMe-TTF-CN-BTD band gap that enables an enhanced photocatalytic hydrogen evolution rate of 122 μmol h^{-1} g^{-1} under visible light. The efficiency of the COOMe-TTF-CN-BTD photocatalyst is also described in terms of medium pH and the nature of the sacrificial agent, where the maximum hydrogen production efficiency is observed at high pH. The findings point to a means of efficient production of hydrogen that can be directly achieved under visible light irradiation without any modifications.

INTRODUCTION

Our growing energy dependence on fossil energy, along with increasing greenhouse gas emissions, has yielded efforts to promote economically viable and alternative resources of energy.[1,2] Hence, it becomes necessary to make a leap in innovative technologies, and reliance on fossil fuels should be restricted. The cyclic carbon-free energies are a great relief for the upcoming demands of energy.[3] In this regard, a hydrogen energy carrier is a key objective in-line with the goal of clean energy resources, which can be obtained easily and in different ways.[4,5] Hydrogen molecules H_2 are able to store and deliver energy, for instance using fuel cells. Because it is not present normally in the atmosphere, it has to be generated from H-rich compounds. It is worth mentioning that hydrogen can be generated by photolysis, electrolysis, or thermal decomposition of water.[6,7] Direct solar water splitting or photolysis processes use light energy to split water into hydrogen and oxygen with the help of a photocatalytic system, which is a one-step way to harness solar energy for hydrogen production.[8]

The extensive variety of photocatalysts, including noble metals and non-noble metals, has been reported to be efficient for the photolytic hydrogen production.[9−13] Among the various materials developed so far, the so-called donor–acceptor (D–A) organic materials have been the focus of interest due to their flexible applications.[14,15] Subsequently, electron–hole separation and charge transfer in D–A materials play a crucial role in high-performance photocatalysis of hydrogen production reaction.[16,17] The A D–A system could accelerate the electron migration and turn the combination of charges down due to direct contacts between donor and acceptor units,[18,19] as also experienced in photovoltaic cells, sensors, and molecular machines.[20,21] With an electron acceptor, such as benzothiadiazole (BTD) linked to the electron donor tetrathiafulvalene (TTF) to form the corresponding D–A system, a charge transfer with the electron–hole pairs occurs.[22] TTF is an electroactive and powerful electron donor that can easily and reversibly be oxidized to its radical cation and di-cation.[23] Such a redox property of TTF is utilized in systems whose structures can be controlled through an external stimulus.[24] Accordingly, the optoelectronic properties of D–A systems, such as TTF–BTD, can be effectively modulated in BTD and TTF units by applying functional groups. In converting solar energy into hydrogen by a photocatalytic system, two principal criteria

Received: August 12, 2022
Accepted: October 24, 2022
Published: November 9, 2022

have to be considered.[25,26] The first is the sunlight absorption by a catalyst, equivalent to or higher than the band gap energy, which generates the electrons and holes.[27,28] The second one is the successful migration of the electron−hole pairs to the catalyst surface before they are recombined together and lose their energy.[29,30]

Herein, we report our recent investigation of the effects of electron-withdrawing and -donating groups on the performance of the TTF−BTD-based photocatalyst for the hydrogen production reaction. Functionalizing NH_2, CH_3, Br, CF_3, COOMe, and CN on the TTF donor part, as well as on the BTD acceptor part, was performed on the corresponding D−A system. The functionalization had a pronounced effect on the molecular orbital energy levels and consequently affects the highest occupied molecular orbital−lowest unoccupied molecular orbital (HOMO−LUMO) gap. Both theoretical and experimental studies were undertaken to better understand the effect of electron-withdrawing and -donating functional groups on the fit of the band gap of the photocatalyst during water splitting reaction. Our results are presented and discussed according to the appropriate modulation of the electron−hole-transfer efficiency and energy levels of TTF−BTDs.

EXPERIMENTAL SECTION

All the chemicals used were of analytical grade and used as received without further purification. TTF−BTD derivative was synthesized by the method that mentioned above.

[1,3]Dithiolo[4′,5′:4,5]benzo[1,2-*c*][1,2,5]thiadiazole-6-thione (1). A solution of thionyl chloride (4.92 g, 41.36 mmol) in dichloromethane (40 mL) was slowly added to a mixture of 5,6-diaminobenzo[*d*][1,3]dithiole-2-thione (3 g, 14 mmol) and triethylamine (25 mL) in dichloromethane (300 mL). After addition, the reaction mixture was heated to reflux for 6 h. The solution was cooled and concentrated in a vacuum followed by trituration in water (100 mL) and the product was extracted with dichloromethane (300 mL). The solvent was removed under reduced pressure and the crude product was recrystallized from ethanol, then solubilized in chloroform (30 mL), and passed through a plug of silica gel to afford [1,3]dithiolo[4′,5′:4,5]benzo[1,2-*c*][1,2,5]thiadiazole-6-thione as a white solid after evaporation of the solvent (2.5 g, 73% yield). mp 148−150 °C. ^{1}H NMR ($CDCl_3$): (δH/ppm) 7.70 (s, 2H). ^{13}C NMR ($CDCl_3$): (δC/ppm) 122.3, 133.3, 152.0, 208.0. FT-IR (ATR): (cm^{-1}) 3040 (Ar−H), 1494 (C═N), 1168 (C−O).

4,8-Dibromo-[1,3]dithiolo[4′,5′:4,5]benzo[1,2-*c*]-[1,2,5] thiadiazole-6-thione (2). Bromine (12.40 g, 77.59 mmol) was added to a solution of [1,3]dithiolo[4′,5′:4,5]-benzo[1,2-*c*][1,2,5]thiadiazole-6-thione (2.42 g, 9.98 mmol) in a mixture of dichloromethane (300 mL) and acetic acid (150 mL), and the reaction mixture was stirred in the dark for 48 h at room temperature. The mixture was then poured into water (400 mL) and extracted with dichloromethane (3 × 200 mL). The combined organic phase was washed with water (200 mL), saturated $NaHCO_3$ (aq) (200 mL), 1 M Na_2SO_3 (aq) (200 mL), and then dried with $MgSO_4$. The solvent was evaporated under reduced pressure and the crude product was recrystallized from ethanol, then solubilized in chloroform (30 mL), and passed through a plug of silica gel to afford 4,8-dibromo-[1,3]dithiolo[4′,5′:4,5]benzo[1,2-*c*][1,2,5]-thiadiazole-6-thione as an off-white solid (2.8 g, 70% yield). mp 138−140 °C. ^{13}C NMR ($CDCl_3$): (δC/ppm) 116.9, 139.2, 158.6, 208.1. FT-IR (ATR): (cm^{-1}) 3100 (Ar−H), 750 (C−Br), 1100 (C−O).

Methyl 2-(4,8-Dibromo-[1,3]dithiolo[4′,5′:4,5]benzo-[1,2-*c*][1,2,5]thiadiazol-6-ylidene)-1,3-dithiole-4-carboxylate (3). Methyl 2-thioxo-1,3-dithiole-4-carboxylate (2 g, 10.4 mmol) was added to a solution of 4,8-dibromo-[1,3]dithiolo [4′,5′:4,5]benzo[1,2-*c*][1,2,5]thiadiazole-6-thione (4 g, 10 mmol) in a triethyl phosphite (50 mL, freshly distilled) and the reaction mixture was stirred for 2 h at 100−105 °C. After cooling to room temperature, the precipitate was collected, washed with methyl alcohol, and dried to give methyl 2-(4,8-dibromo-[1,3]dithiolo[4′,5′:4,5]benzo[1,2-*c*]-[1,2,5]thiadiazol-6-ylidene)-1,3-dithiole-4-carboxylate (3.8 g, 69%). mp 163−165 °C. ^{1}H NMR ($CDCl_3$): (δH/ppm) 3.70 (s, 3H), 8.1 (s, 1H). ^{13}C NMR ($CDCl_3$): (δC/ppm) 51.1, 111.3, 116.0, 132.0, 133.3, 138.0, 139.1, 139.4, 158.1, 168.0. FT-IR (ATR): (cm^{-1}) 3010 (Ar−H), 1510 (C═N), 1170 (C−O), 765 (C−Br).

Methyl 2-(4,8-Dicyano-[1,3]dithiolo[4′,5′:4,5]benzo-[1,2-*c*][1,2,5]thiadiazol-6-ylidene)-1,3-dithiole-4-carboxylate (COOMe-TTF-CN-BTD) (4). In a 100 ml, three-necked, round flask fitted with a sealed stirrer, a thermometer, and a reflux condenser, were placed methyl 2-(4,8-dibromo-[1,3]dithiolo[4′,5′:4,5]benzo[1,2-*c*][1,2,5]thiadiazol-6-ylidene)-1,3-dithiole-4-carboxylate (5.2 g, 10 mmol), cuprous cyanide (3.0 g, 33.5 mmol), of pyridine (5.0 mL). The contents were then heated to 180 °C in 15 min while being stirred well; then contents were maintained for 6 h at 180 °C. After the required time, the contents were cooled to room temperature, and a brownish complex of the CuBrBase was precipitated from the solution. A part of the solution containing benzonitrile and passed through a plug of silica gel to afford a yellow solid of methyl 2-(4,8-dicyano-[1,3]dithiolo[4′,5′:4,5]benzo[1,2-*c*][1,2,5]thiadiazol-6-ylidene)-1,3-dithiole-4-carboxylate (2.8 g, 66%). mp 170−173 °C. FT-IR ν_{max} (neat): 3332, 3150, 2219, 1700, 1650, 1554, 1414, 739 cm^{-1}. ^{1}H NMR ($CDCl_3$, 500 MHz): δ 8.10 (s, 1H), 3.79 (s, 3H) ppm. ^{13}C NMR ($CDCl_3$,125 MHz): δ 167.9, 157.2, 139.4, 138.2, 134.1, 132.2, 111.5, 116.0, 111.2, 110.8, 50.9 ppm.

Photocatalytic Measurements. We used an immersion-type reactor (Lelesil innovative systems, India) for carrying the photocatalytic experiments. All the reactions were carried out without any noble metals as a co-catalyst. Reactions were done using double distilled water (500 mL) in the presence of a photocatalyst (0.5 g/L) and sacrificial reagent (10% V/V). First of all, the mixture was stirred for 1 h under nitrogen purging then was irradiated under a solar light source (300WXenon arc lamp). At least the photocatalyst was filtered (0.45 μm micro-filter) and analyzed to measure the photocatalyst structure changes. Besides, we used Agilent gas chromatography with a thermal conductivity detector to investigate hydrogen gas production.

Characterization. The UV−visible diffuse reflectance spectra were recorded in the range from 900 to 200 nm using a Shimadzu UV-3600. For this, 0.001 g sample was dispersed in 5 mL of ethanol and further ultrasonicated for half hour to obtain transparent colloidal solutions. Also, Fourier transform infrared spectroscopy (FTIR, PerkinElmer, USA) was used to characterize the products based on the measurement of the absorption of electromagnetic radiation with wavelengths within the mid-infrared region (4000−400 cm^{-1}). We used the attenuated total reflection (ATR) method

https://doi.org/10.1021/acsomega.2c05185
ACS Omega 2022, 7, 42283−42291

Scheme 1. Synthesis Process and Functionalization of TTF−BTD-Based Photocatalysts

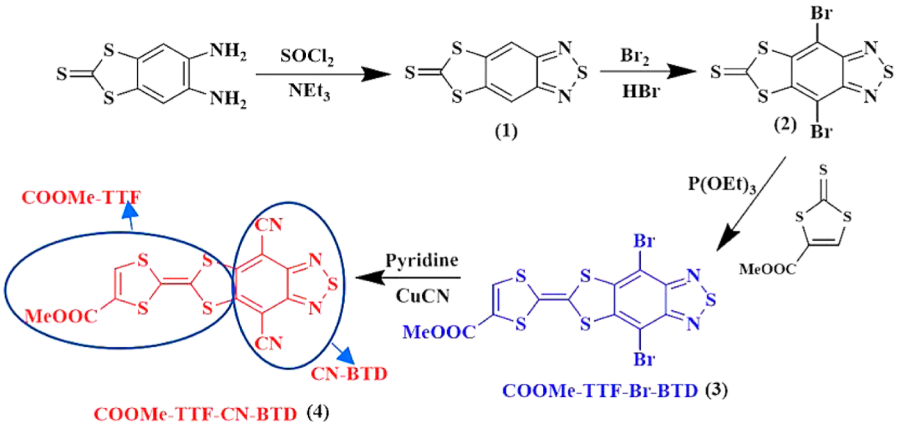

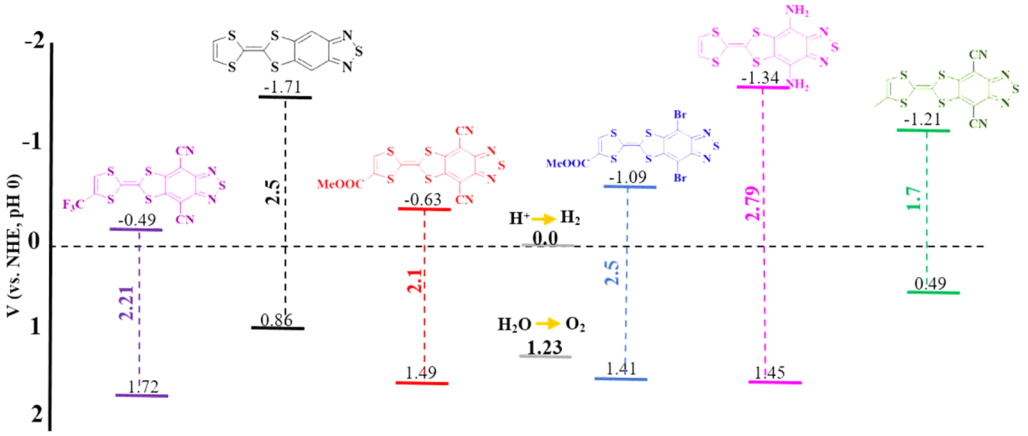

Figure 1. Energy diagram of the TTF−BTD derivatives. NHE, normal hydrogen electrode.

that allows the direct measurement of powder samples. NMR spectra were recorded on a Bruker Avance DPX-400 and 500. For this, 0.01 g sample was dissolved in deuterated chloroform ($CDCl_3$), any residual water in the solvent is removed by the addition of activated 4 Å molecular sieves.

The purity of the products and the progress of the reactions were determined and established by TLC on silica-gel Polygram SILG/UV254 plates or by a Shimadzu Gas Chromatograph GC-14A instrument with a flame ionization detector. Electrochemical measurements were carried out in a three electrode cell system by using a CHI760E electrochemical work station (Chenhua, Shanghai), where indium thin oxide deposited with samples as the working electrode, Ag/AgCl electrode as the reference electrode, and Pt flake as the counter electrode. Gaussian 09 program package was employed for calculating the electronic structures of ground and excited states of the model structures. The geometries of the ground states were optimized with density functional theory (DFT), and TDDFT was applied for the calculation of vertical excited energies. The B3LYP functional and 6-311G(d,p) basis sets were used in the calculation. The polarizable continuum model (PCM) was used to simulate the solvation effect. The dielectric constant of the solvent was set to 73.

RESULTS AND DISCUSSION

The TTF−BTDs were synthesized by a cycloaddition reaction to prepare the BTD moiety, followed by a coupling reaction for the TTF part (as a Scheme 1).[31] For the first step, we used freshly distilled thionyl chloride in the presence of a base. The BTD was converted to Br-BTD by the reaction with molecular bromine (added dropwise very slowly) in hydrobromic acid. Afterward, the TTF part was synthesized with the triethyl phosphite-mediated coupling reaction. At last, COOMe-TTF-Br-BTD in the presence of copper cyanide and pyridine successfully converts to COOMe-TTF-CN-BTD.[32] The high purity of the products in any step was achieved by easy purification using a standard chromatographic technique or crystallization. Finally, the characterization of the compounds was fully achieved (Figures S1−S7, Supporting Information). The CNMR, HNMR, and FTIR analysis of compounds 1, 2, 3, and 4 have proved the purity and their structure. As shown in Figures S1−S7, the spectra in region 3000−3100 cm^{-1} show the hydrogen groups of aromatics. In addition, the band at 1450−1500 cm^{-1} is due to C−N stretching vibration in aromatic carbons. The peak at 1160−1200 cm^{-1} is attributed to C−O stretching vibration in aromatic carbons.

The structure of donor−acceptor couples in TTF−BTDs is established by applying Gaussian 09 theoretical calculations.[33] The HOMO shows its major electron density lodging on the TTF part, while the LUMO is located on the BTD moiety (Figure 1). This suggests that the electrons can be generated by exciting the electron donor part of the TTF unit. It is found that the stronger electron-withdrawing functional group on TTF−BTD has remarkable effects on band gap. In order to induce changes in the electronic properties, functional groups

https://doi.org/10.1021/acsomega.2c05185
ACS Omega 2022, 7, 42283−42291

(Br, CN, COOMe, CF_3, CH_3, and NH_2) were added to the TTF−BTD structures. A change in the HOMO and LUMO energy levels was observed in the order CH_3 < Br < CF_3 < COOMe < CN.

Also, the reduction and oxidation energies of H_2O were calculated by ab initio thermodynamics to check whether they are located inside the photocatalyst band gap. According to the databases, the reduction potential of hydrogen (H^+ to H_2) is 4.18 eV and the oxidation potential of H_2O to O_2 is 5.30 eV. The energy contrast between the oxygen and hydrogen evolution potentials is 1.229 eV. Consequently, the conduction and valence bands of the ideal photocatalysts have to be located favorably, so that they stand astride over the hydrogen and oxygen evolution potentials. The results discover the potential of COOMe-TTF-CN-BTD, which can have the photocatalytic power in inducing hydrogen production. The COOMe-TTF-CN-BTD is able to overcome these potentials, which is referred to have a band gap of 1.8−2.0 eV for hydrogen production in sunlight.[34] As shown in Figure 1, the reduction level for H^+ is well positioned under the conductive band, and the oxidation level is located above the valence band of COOMe-TTF-CN-BTD.

The calculated band gap for COOMe-TTF-Br-BTD molecule is 2.5 eV, which decreases to 2.1 eV for COOMe-TTF-CN-BTD when substituting Br by the CN group, with the density functional theory that is in support of UV−vis analysis (Table S1). This affirms that the BTD moiety is favorable for oxidation sites of H_2O to O_2, whereas the reduction sites for H^+ to H_2 would be on the TTF part (Figure 2). The sunlight excites the electrons to the conduction band,

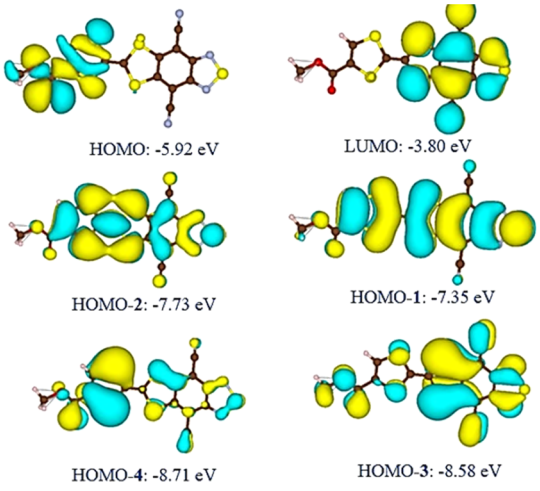

Figure 2. Illustration of the molecular orbitals of CN-TTF-BTD.

so holes are created in the valence band. It is noteworthy that COOMe-TTF-CN-BTD has a narrow band gap and is able to absorb visible light and generate electrons and holes in photocatalytic processes.

The electrochemical properties of TTF−BTD derivatives were demonstrated by cyclic voltammetry in acetonitrile (0.1 mM $NaPF_6$ solution), with a scan rate of 100 mV/s (Figure 3). COOMe-TTF-Br-BTD has two reversible reduction and oxidation waves at $E_{1/2}^{Red1}$ = −0.48 V and $E_{1/2}^{Red2}$ = −1.18 V and $E_{1/2}^{OX1}$ = 0.78 V and $E_{1/2}^{OX2}$ = 1.45 V (vs Ag/AgCl); corresponding to the replacing Br groups on BTD with CN groups, the reduction and oxidation waves of COOMe-TTF-CN-BTD are changed to $E_{1/2}^{Red1}$ = −0.57 V and $E_{1/2}^{Red2}$ = −1.49 V and $E_{1/2}^{OX1}$ = 0.95 V and $E_{1/2}^{OX2}$ = 1.57 V (vs Ag/AgCl). The peaks associated with COOMe-TTF-CN-BTD approximately 0.5 V shifted toward higher potentials in contrast with the core TTF−BTD ($E_{1/2}^{OX1}$ = 0.38 V and $E_{1/2}^{OX2}$ = 0.87 V). As demonstrated, the electron-withdrawing property of CN and COOMe functional groups affects the exchange current density and electrochemical oxidation reaction rate.

The UV−vis spectroscopy is used to measure the number of discrete wavelengths of ultraviolet and visible light absorbed by the samples (Figure 4). It is shown that the absorption band 285−500 nm is allocated to the TTF−BTD excited states. Besides, a medium-intense band is observed at 510−570 nm, which is in the visible region. This phenomenon is attributed to a singlet intramolecular charge transfer η to η^*. The covalently linkage of TTF (donor) and benzothiazine (acceptor) plays an important role in the modulation of intramolecular charge-transfer and photophysical properties). On the other hand, the UV−vis analysis results proved that the replacement of Br with CN reduces the band gap, which is attributed to the more electron-withdrawing effect of CN. The band gap of the COOMe-TTF-CN-BTD obtained from UV−vis results is 2.1 eV. It is confirmed that the band gap of the photocatalyst in hydrogen production should be larger than the standard Gibbs free energy change of water splitting (1.23 eV, ΔG = + 237.2 kJ mol^{-1}). Moreover, the conduction band should be lower than the water reduction, and the valence band has to be higher than water oxidation.

The photocatalytic hydrogen production reaction in the powder form was investigated over several systems in the presence of TTF−BTD derivatives (Figure 5). The hydrogen is created from water by using triethanolamine (TEOA) as a sacrificial electron donor and TTF−BTD derivative photocatalyst in light illumination and absence of noble metal catalysts. The total amount of hydrogen generated at the first run for COOMe-TTF-CN-BTD, CN-TTF-Br-BTD, and TTF−BTD is around 360, 25, and 13 μmol, respectively. These results indicate that COOMe-TTF-CN-BTD acts as a "metal-free" photocatalyst for hydrogen production in visible light. The COOMe-TTF-CN-BTD powder is insoluble in water as well as in acidic (HCl, pH = 1) or base (NaOH, pH = 8) media. Although the hydrogen evolution rate decreased moderately in each run, the activity is reintroduced by adding a satisfied agent. Also, the elemental analysis of COOMe-TTF-CN-BTD after four cycles of photoreaction proves that it is a stable compound (C, 39.90%; H, 0.97%; N, 13.21%; O, 7.72%; and S, 38.12%).

The COOMe-TTF-CN-BTD efficiency as a photocatalyst was measured in various medium pH and different sacrificial agents. Also, hydrogen production is investigated in the absence of the photocatalyst, only sacrificial reagents under solar light irradiation. It is noteworthy that hydrogen is generated in high alkaline (TEOA) and acidic (lactic acid) media, contrasting to the neutral pH (Figure 6). We use TEOA to create the high pH due to being a strong base, and also the fact that it can act as a sacrificial agent (1% solution has a pH of approximately 10). The total amounts of hydrogen produced with COOMe-TTF-CN-BTD photocatalyst in acidic media (pH = 2) and alkalic media (pH = 10) is around 67 and 40 μmol, respectively. These results indicate that COOMe-TTF-CN-BTD acts as a stable "metal-free" photocatalyst in acidic or alkali media.

The hydrogen generation and oxygen evolution are referred to the photo-electro-chemical reactions on COOMe-TTF-CN-

https://doi.org/10.1021/acsomega.2c05185
ACS Omega 2022, 7, 42283−42291

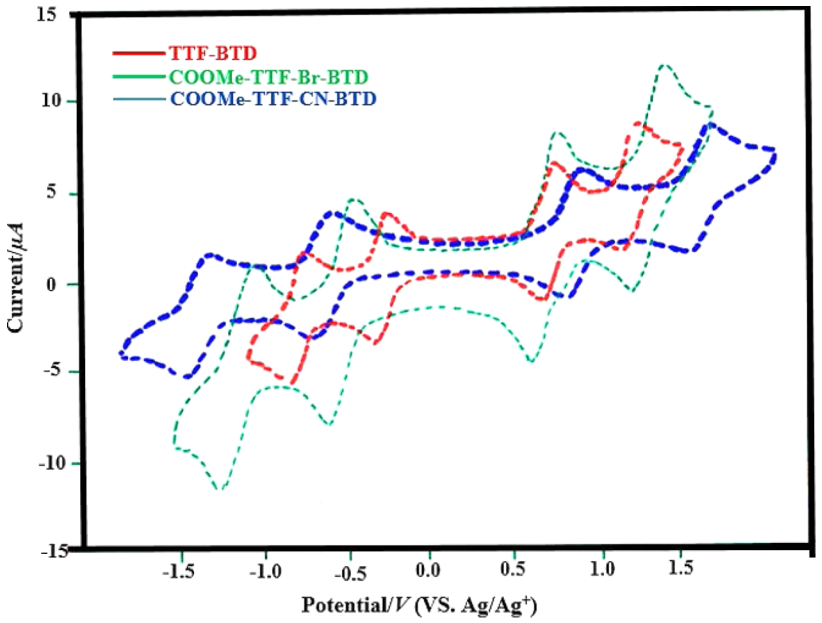

Figure 3. Cyclic voltammograms of COOMe-TTF-CN-BTD, COOMe-TTF-Br-BTD, and TTF−BTD derivatives.

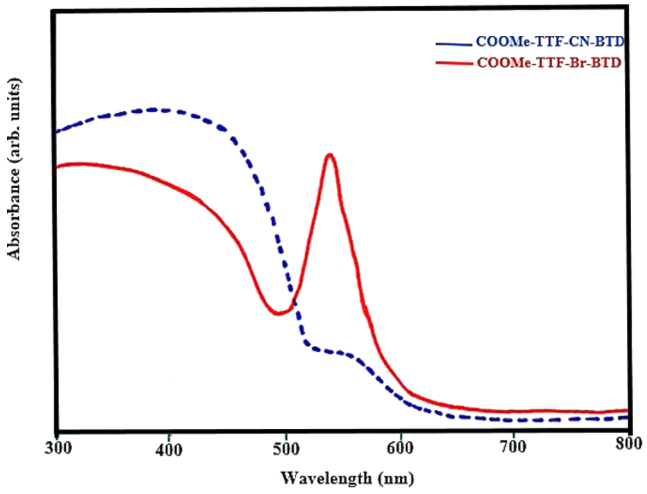

Figure 4. Ultraviolet−visible diffuse reflectance spectrum of the COOMe-TTF-CN-BTD and COOMe-TTF-Br-BTD.

BTD photocatalysts in visible light, which occur simultaneously, as shown in Scheme 2. With regard to the alkaline media, at first, the catalyst needs to break the H−O−H via photo-electro-chemical reduction of H_2O. The adsorbed H combines with the hydrated proton and then receives an electron from the catalyst surface to form H_2. On the other hand, the OH anion gives out an electron and chemically attaches onto the catalyst, while the adsorbed oxygen generated after the second electron is removed and accompanies the formation of a H_2O molecule. Finally, two adsorbed oxygen bonds to each other to produce O_2. In fact, the hydroxide anion can provide easily in alkaline media so is beneficial for oxygen evolution; on the other hand, the electron is flowing in the system and hydrogen generation is going well.

The evidence shows that the TTF moiety of COOMe-TTF-CN-BTD is able to reform in acid media by H^+, which protonate the central C═C double bond and create $HTTF^+$ (6) (as shown in Scheme 3). $HTTF^+$ can also react with another COOMe-TTF-CN-BTD (5) molecule and then by the radical-substrate coupling reaction, it can produce two TTF-based radicals (7) and (8). It is shown that the H^+ acts as an electron acceptor, so the COOMe-TTF-CN-BTD efficiency in an acidic media will reduce in contrast to alkali media, which is a more efficient media for hydrogen production.

COOMe-TTF-CN-BTD is stable in both acidic and alkaline solutions during hydrogen production. The photocatalytic hydrogen production efficiency of COOMe-TTF-CN-BTD is investigated in various sacrificial agents (as shown in Figure 7). The sacrificial agents that we used include TEOA, ethylene glycol (EG), Na_2S/Na_2SO_3, and lactic acid in the hydrogen generation reaction. The COOMe-TTF-CN-BTD/TEOA system showed the maximum efficiency (360.2 μmol) in hydrogen production. The efficiencies of COOMe-TTF-CN-BTD/lactic acid, COOMe-TTF-CN-BTD/EG, and COOMe-TTF-CN-BTD/Na_2S/Na_2SO_3 systems was found to be 184, 35.4, and 30.8 μmol, respectively.

To study the water dispersity of COOMe-TTF-CN-BTD, no dispersion stabilizer was used to investigate the re-aggregation of the photocatalyst in water (Figure S8). Due to the hydrogen bonding interaction between COOMe-TTF-CN-BTD and water in alkaline media, more uniform and stable dispersion was obtained, without aggregation and precipitation over 1 day at a concentration of ∼1 mg mL^{-1}, and was used for hydrogen production application. The reusability and stability of photocatalysts were studied, as shown in below Figure 8. The reused photocatalyst shows no deterioration of hydrogen production reaction after being used in five runs. After each run, the photocatalyst was separated via centrifugation and dried at 80 °C for 12 h (all the reaction parameters were kept constant), and the catalyst were reused for 5 testing runs. The hydrogen production has the same range even with a reusability of five times, indicating that the catalyst has a high stability.

Note, as compared to the reported D−A-conjugated molecules, the small molecule of COOMe-TTF-CN-BTD semiconductor exhibited a well-defined structure and uniform nature. This molecule also represented high thermal and chemical stability and high-water dispersion, without any costly

https://doi.org/10.1021/acsomega.2c05185
ACS Omega 2022, 7, 42283−42291

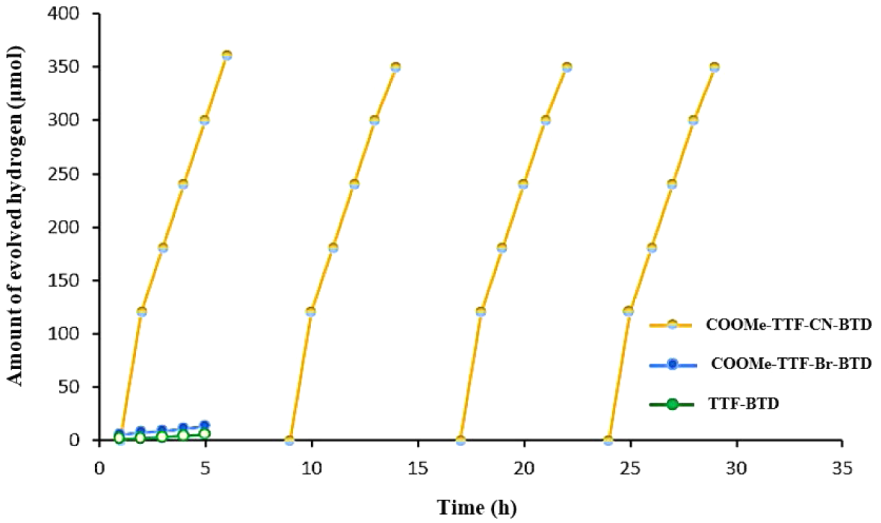

Figure 5. Photocatalytic hydrogen evolution of the COOMe-TTF-CN-BTD, COOMe-TTF-Br-BTD, and TTF−BTD derivatives.

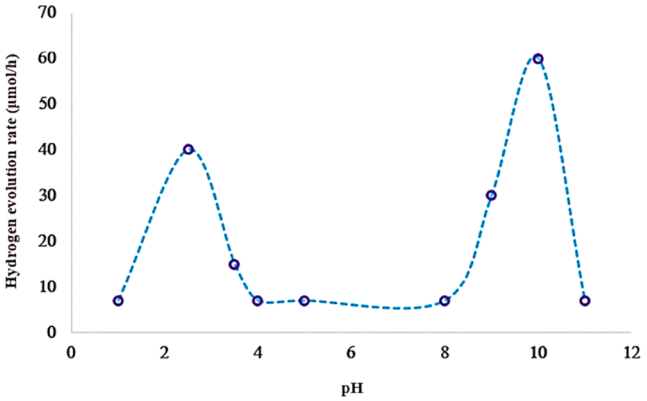

Figure 6. Effect of the medium pH on the photocatalytic hydrogen evolution in the presence of the COOMe-TTF-CN-BTD photocatalyst.

and energy-consuming processes such as high-temperature and pressure conditions during the synthesis processes; therefore, it holds promise for scaling-up and industrial application. Also, the catalyst quantum efficiency (η) over 5 h of visible light irradiation was calculated as the ratio of the number of hydrogen molecules produced to the number of photons interacting with the sample (the transfer of two electrons is required to produce one hydrogen molecule), 5.4% at 480 nm. This indicates that the COOMe-TTF-CN-BTD exhibits good photocatalytic activity for photocatalytic hydrogen production under visible light in the absence of a noble metal.

CONCLUSIONS

In this work, we presented the TTF−benzothiadiazole derivative, COOMe-TTF-CN-BTD, as a simple and stable photocatalyst that yields the stable dispersion of the photocatalyst in water and enables one to generate hydrogen from water in the absence of noble metals. We adopted various

Scheme 2. Photo-electro-chemical Mechanism of Hydrogen Generation and Oxygen Evolution on the COOMe-TTF-CN-BTD Photocatalyst in Alkaline Media

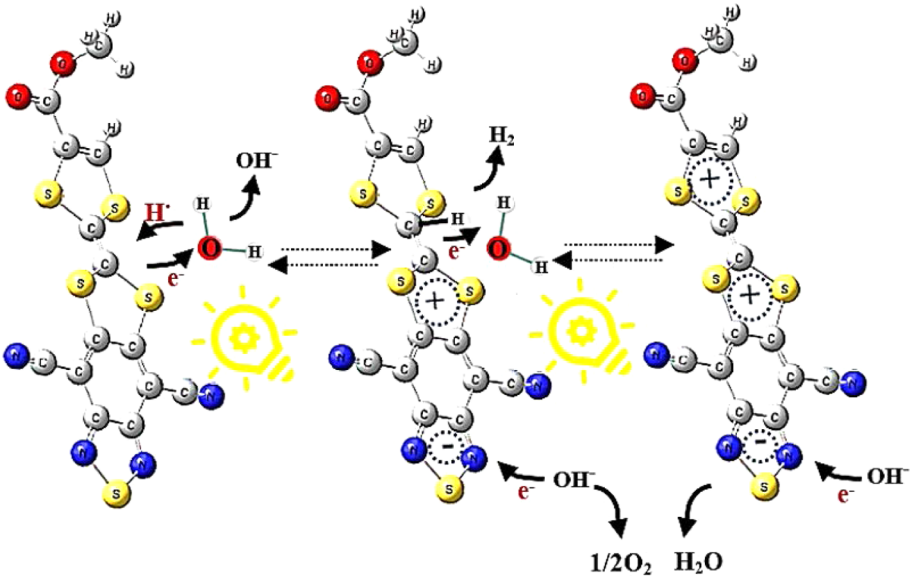

https://doi.org/10.1021/acsomega.2c05185
ACS Omega 2022, 7, 42283−42291

Scheme 3. COOMe-TTF-CN-BTD Variations in Acidic Media

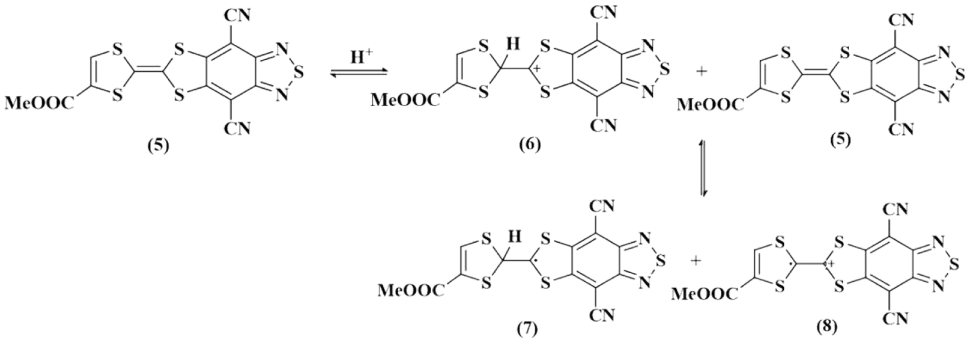

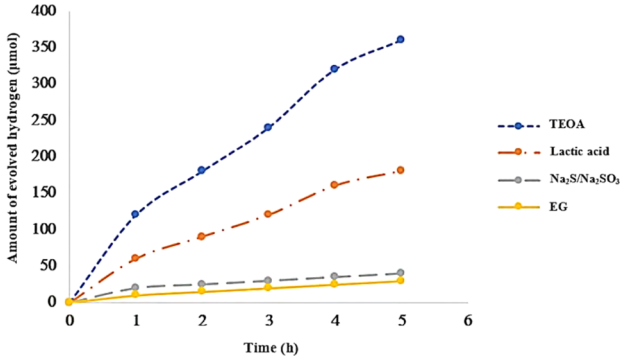

Figure 7. Photocatalytic H_2 production efficiency of COOMe-TTF-CN-BTD using various sacrificial agents.

functional groups, such as NH_2, CH_3, Br, CF_3, COOMe, and CN on the TTF−BTD to investigate the band gap variations. Also, the effect of different sacrificial agents and pH media was studied. The results of the band structure indicate that the pure TTF−BTD shows 2.5 eV band gap while the electron-donating groups can open the gap of TTF−BTD by 2.79 eV. On the other hand, it was shown that the electron-withdrawing groups, CN and COOMe, can lead to the most suitable variations of system band gap by 2.1 eV. The COOMe-TTF-CN-BTD exhibited a much-enhanced hydrogen evolution reaction than COOMe-TTF-Br-BTD. Furthermore, the COOMe-TTF-CN-BTD represented enhanced kinetics for the hydrogen evolution reaction in contact with alkaline solution relative to acidic solution. It was found clearly that COOMe-TTF-CN-BTD/TEOA is the best system with maximum hydrogen production in this study. The present results provide new insights for the practical application of water splitting in a scalable and economically feasible way, by making use of the thermally and oxidation-stable organic semiconductor structure as the donor−acceptor materials.

■ ASSOCIATED CONTENT

Supporting Information

The Supporting Information is available free of charge at https://pubs.acs.org/doi/10.1021/acsomega.2c05185.

Band gap, HOMO, and LUMO energies study, CNMR and HNMR analyses, and water-dispersity of COOMe-TTF-CN-BTD (PDF)

■ AUTHOR INFORMATION

Corresponding Authors

Hajar Mahmoudi − *Department of Photonics, Graduate University of Advanced Technology, Kerman 7631885356, Iran;* orcid.org/0000-0002-0334-6635; Email: mahmoudi.hajar@gmail.com

Abdel El Kharbachi − *Helmholtz Institute Ulm (HIU), Ulm 89081, Germany;* orcid.org/0000-0003-4332-1544; Email: kharbachi@kit.edu

Authors

Hassan Safari − *Department of Photonics, Graduate University of Advanced Technology, Kerman 7631885356, Iran*

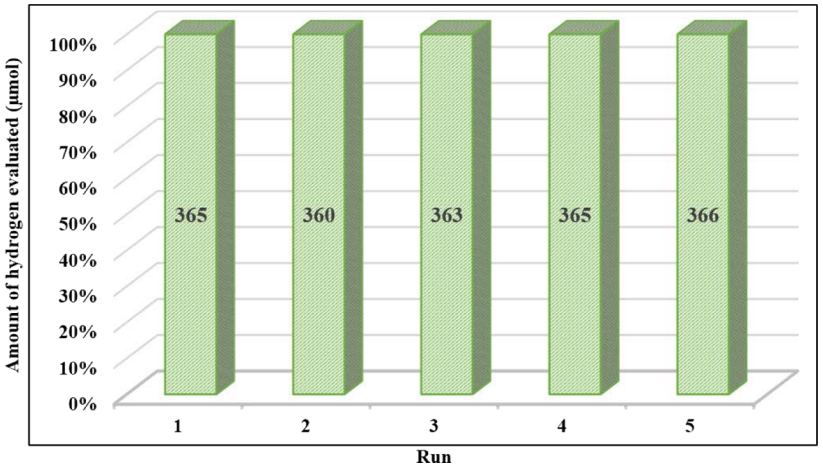

Figure 8. Reusability and stability of COOMe-TTF-CN-BTD after five consecutive runs.

https://doi.org/10.1021/acsomega.2c05185
ACS Omega 2022, 7, 42283−42291

Abbas Ali Jafari − *Department of Chemistry, Yazd University, Yazd 89195-741, Iran*

Complete contact information is available at: https://pubs.acs.org/10.1021/acsomega.2c05185

Notes

The authors declare no competing financial interest.

The original data in this work is available from the corresponding author upon reasonable requests.

■ ACKNOWLEDGMENTS

H.M. and H.S. are grateful to the partial support of Iran Science Elites Federation. A.A.J. thanks to the Research Council of Yazd University for financial support.

■ REFERENCES

(1) Cao, H.; Zhang, Z.; Zhang, M.; Gu, A.; Yu, H.; Ban, H.; Sun, Q.; Shen, Y.; Zhang, X.-L.; Zhu, J.; Wang, M. The effect of defects in tin-based perovskites and their photovoltaic devices. *Mater. Today Phys.* **2021**, *21*, 100513.

(2) Luo, D.; Ren, Z. Synthesis of sodium nanoparticles for promising extraction of heavy oil. *Mater. Today Phys.* **2021**, *16*, 100276.

(3) Vyas, V. S.; Haase, F.; Stegbauer, L.; Savasci, G.; Podjaski, F.; Ochsenfeld, C.; Lotsch, B. V. A tunable azine covalent organic framework platform for visible light-induced hydrogen generation. *Nat. Commun.* **2015**, *6*, 8508.

(4) Bartela, Ł. A hybrid energy storage system using compressed air and hydrogen as the energy carrier. *Energy* **2020**, *196*, 117088.

(5) Sazali, N. Emerging technologies by hydrogen: A review. *Int. J. Hydrogen Energy* **2020**, *45*, 18753−18771.

(6) Shi, X.; Liao, X.; Li, Y. Quantification of fresh water consumption and scarcity footprints of hydrogen from water electrolysis: A methodology framework. *Renewable Energy* **2020**, *154*, 786−796.

(7) Safari, F.; Dincer, I. A review and comparative evaluation of thermochemical water splitting cycles for hydrogen production. *Energy Convers. Manage.* **2020**, *205*, 112182.

(8) Li, R. Latest progress in hydrogen production from solar water splitting via photocatalysis, photoelectrochemical, and photovoltaic-photoelectrochemical solutions. *Chin. J. Catal.* **2017**, *38*, 5−12.

(9) Yang, M.-Q.; Han, C.; Xu, Y.-J. Insight into the effect of highly dispersed MoS2 versus layer-structured MoS2 on the photocorrosion and photoactivity of CdS in graphene−CdS−MoS2 composites. *J. Phys. Chem. C* **2015**, *119*, 27234−27246.

(10) Yuan, L.; Han, C.; Yang, M.-Q.; Xu, Y.-J. Photocatalytic water splitting for solar hydrogen generation: fundamentals and recent advancements. *Int. Rev. Phys. Chem.* **2016**, *35*, 1−36.

(11) Han, B.; Liu, S.; Zhang, N.; Xu, Y.-J.; Tang, Z.-R. One-dimensional CdS@ MoS2 core-shell nanowires for boosted photocatalytic hydrogen evolution under visible light. *Appl. Catal., B* **2017**, *202*, 298−304.

(12) Li, Y.-H.; Qi, M.-Y.; Li, J.-Y.; Tang, Z.-R.; Xu, Y.-J. Noble metal free CdS@ CuS-NixP hybrid with modulated charge transfer for enhanced photocatalytic performance. *Appl. Catal., B* **2019**, *257*, 117934.

(13) Qi, M.-Y.; Conte, M.; Anpo, M.; Tang, Z.-R.; Xu, Y.-J. Cooperative coupling of oxidative organic synthesis and hydrogen production over semiconductor-based photocatalysts. *Chem. Rev.* **2021**, *121*, 13051−13085.

(14) Lan, Z.-A.; Ren, W.; Chen, X.; Zhang, Y.; Wang, X. Conjugated donor-acceptor polymer photocatalysts with electron-output "tentacles" for efficient hydrogen evolution. *Appl. Catal., B* **2019**, *245*, 596−603.

(15) Zhou, W.; Hu, Z.; Huang, F.; Hong, W.; Chen, X. Metal-free hydrophilic D-A conjugated polyelectrolyte dots/g-C3N4 nanosheets heterojunction for efficient and irradiation-stable water-splitting photocatalysis. *Appl. Catal., B* **2020**, *270*, 118852.

(16) Guo, L.; Niu, Y.; Xu, H.; Li, Q.; Razzaque, S.; Huang, Q.; Jin, S.; Tan, B. Engineering heteroatoms with atomic precision in donor−acceptor covalent triazine frameworks to boost photocatalytic hydrogen production. *J. Mater. Chem. A* **2018**, *6*, 19775−19781.

(17) Ai, M.; Zhang, J.-W.; Gao, R.; Pan, L.; Zhang, X.; Zou, J.-J. MnOx-decorated 3D porous C3N4 with internal donor−acceptor motifs for efficient photocatalytic hydrogen production. *Appl. Catal., B* **2019**, *256*, 117805.

(18) Lan, X.; Li, Q.; Zhang, Y.; Li, Q.; Ricardez-Sandoval, L.; Bai, G. Engineering donor-acceptor conjugated organic polymers with boron nitride to enhance photocatalytic performance towards visible-light-driven metal-free selective oxidation of sulfides. *Appl. Catal., B* **2020**, *277*, 119274.

(19) Jiang, R.; Lu, G.; Liu, J.; Wu, D.; Yan, Z.; Wang, Y. Incorporation of pi-conjugated molecules as electron donors in g-C3N4 enhances photocatalytic H_2-production. *Renewable Energy* **2021**, *164*, 531−540.

(20) Ma, L.; Yao, H.; Wang, J.; Xu, Y.; Gao, M.; Zu, Y.; Cui, Y.; Zhang, S.; Ye, L.; Hou, J. Impact of Electrostatic Interaction on Bulk Morphology in Efficient Donor−Acceptor Photovoltaic Blends. *Angew. Chem.* **2021**, *133*, 16124−16130.

(21) Yao, Y.; Xu, H.-L.; Su, Z.-M. The second-order NLO and TADF properties of a donor−acceptor dihydropyrene−cyclophanediene system: the impact of molecular architecture and polarizable environment. *J. Mater. Chem. C* **2022**, *10*, 886−898.

(22) Bergkamp, J. J.; Decurtins, S.; Liu, S.-X. Current advances in fused tetrathiafulvalene donor−acceptor systems. *Chem. Soc. Rev.* **2015**, *44*, 863−874.

(23) Segura, J. L.; Martín, N. New concepts in tetrathiafulvalene chemistry. *Angew. Chem., Int. Ed.* **2001**, *40*, 1372−1409.

(24) Goeb, S.; Sallé, M. Electron-rich Coordination Receptors Based on Tetrathiafulvalene Derivatives: Controlling the Host−Guest Binding. *Acc. Chem. Res.* **2021**, *54*, 1043−1055.

(25) Ahmad, H.; Kamarudin, S.; Minggu, L.; Kassim, M. Hydrogen from photo-catalytic water splitting process: A review. *Renewable Sustainable Energy Rev.* **2015**, *43*, 599−610.

(26) Peng, Q.; Xiong, R.; Sa, B.; Zhou, J.; Wen, C.; Wu, B.; Anpo, M.; Sun, Z. Computational mining of photocatalysts for water splitting hydrogen production: two-dimensional InSe-family monolayers. *Catal. Sci. Technol.* **2017**, *7*, 2744−2752.

(27) Hammarström, L. Accumulative charge separation for solar fuels production: coupling light-induced single electron transfer to multielectron catalysis. *Acc. Chem. Res.* **2015**, *48*, 840−850.

(28) Wang, H.; Zhang, J.; Yuan, X.; Jiang, L.; Xia, Q.; Chen, H. Photocatalytic removal of antibiotics from natural water matrices and swine wastewater via Cu (I) coordinately polymeric carbon nitride framework. *Chem. Eng. J.* **2020**, *392*, 123638.

(29) Wang, H.; Qian, C.; Liu, J.; Zeng, Y.; Wang, D.; Zhou, W.; Gu, L.; Wu, H.; Liu, G.; Zhao, Y. Integrating suitable linkage of covalent organic frameworks into covalently bridged inorganic/organic hybrids toward efficient photocatalysis. *J. Am. Chem. Soc.* **2020**, *142*, 4862−4871.

(30) Sarkar, O.; Katakojwala, R.; Venkata Mohan, S. Low carbon hydrogen production from a waste-based biorefinery system and environmental sustainability assessment. *Green Chem.* **2021**, *23*, 561−574.

(31) Rohwer, E. J.; Akbarimoosavi, M.; Meckel, S. E.; Liu, X.; Geng, Y.; Lawson Daku, L. M.; Hauser, A.; Cannizzo, A.; Decurtins, S.; Stanley, R. J.; et al. Dipole Moment and Polarizability of Tunable Intramolecular Charge Transfer States in Heterocyclic π-Conjugated Molecular Dyads Determined by Computational and Stark Spectroscopic Study. *J. Phys. Chem. C* **2018**, *122*, 9346−9355.

(32) Wang, D.; Han, H.; Gao, H.; Yang, Z.; Xing, Y.; Cao, H.; He, W.; Wang, H.; Gu, J.; Hu, H. Synthesis and evaluation of simple molecules for dye sensitized solar cells. *Synth. Met.* **2016**, *220*, 41−47.

(33) Treutler, O.; Ahlrichs, R. Efficient molecular numerical integration schemes. *J. Chem. Phys.* **1995**, *102*, 346−354.

(34) Razek, S. A.; Popeil, M. R.; Wangoh, L.; Rana, J.; Suwandaratne, N.; Andrews, J. L.; Watson, D. F.; Banerjee, S.;

Piper, L. F. J. Designing catalysts for water splitting based on electronic structure considerations. *Electron. Struct.* **2020**, *2*, 023001.

https://doi.org/10.1021/acsomega.2c05185
ACS Omega 2022, 7, 42283−42291